A new modal correction method for linear structures subjected to deterministic and random loadings

Alessandro Palmeri[a,*], Mariateresa Lombardo[b]

[a] *Department of Civil and Building Engineering, Loughborough University, Sir Frank Gibb Building, Loughborough LE11 3TU, United Kingdom*
[b] *Department of Civil and Structural Engineering, University of Sheffield, Sir Frederick Mappin Building, Sheffield S1 3JD, United Kingdom*

Abstract

In the general framework of linear structural dynamics, modal corrections methods allow improving the accuracy of the response evaluated with a reduced number of modes. Although very often neglected by researchers and practitioners, this correction is particularly important when strains and stresses are computed. Aimed at overcoming the main limitations of existing techniques, a novel dynamic modal acceleration method (DyMAM) is presented and numerically validated. The proposed correction involves a set of additional dummy oscillators, one for each dynamic loading, and can be applied, with a modest computational effort, to discrete and continuous systems under deterministic and random inputs.

Keywords: earthquake engineering, modal correction, modal acceleration method (MAM), random vibration, sensitivity analysis, structural dynamics

1. Introduction

The vast majority of civil engineering structures exposed to dynamic actions like wind gusts, ground shakings and moving loads are designed with the help of the modal analysis, in so reducing the size of the structural problem, and therefore the computational effort. This leads to the classical truncation procedure known to the literature as modal displacement method (MDM), in which a reduced set of natural modes of vibrations is used to calculate the response of the system. The downside of this procedure is the unavoidable loss of accuracy associated with the truncation of high-frequency modes, whose contribution is not retained in the analysis. In the current state of practice, the truncation is generally accepted if the sum of the effective modal masses participating in the motion exceeds a given threshold, e.g. 90% of the total mass of the structure (as in the European seismic code [1]). Even though dependable by many researchers and practitioners, this criterion may fail in terms of strains and stresses, introducing large inaccuracies in the design values for strength and fatigue checks. Hence, it clearly emerges the practical importance of methods able to correct the modal response in such a way to achieve the required accuracy. This is generally done by adding to the MDM solution an approximate contribution somehow related to the higher modes.

The most popular modal correction technique is the so-called mode acceleration method (MAM), in which the adjustment is simply given by the pseudo-static contribution of the higher modes of vibration [2, 3]. This procedure has been also extended to cope with random loadings represented via Karhunen-Loève decomposition [4].

Even though straightforward, the accuracy of the MAM reduces when the dynamic loadings have a significant high-frequency content. Improved results can be obtained with the force derivative methods (FDM), whose correction is built as a series expansion [5, 6]. This requires the knowledge of successive time derivatives of the excitation, which are not always available, therefore limiting the practical applicability of the method.

A different approach underlies the dynamic correction method (DCM), in which the particular solutions of the differential equations ruling the motion in both geometrical and modal space are used to define the corrective term [7]. Originally formulated for dynamic loadings represented by analytical expressions, e.g. harmonic functions, this technique has been extended to cope with piecewise linear excitations, e.g. recorded accelerograms. The mathematical derivation of this improved DCM (IDCM) can be found in reference [8], where it is also shown that MAM and FDM can be viewed as particular cases of the DCM.

In the attempt of mitigating the computational effort, a corrective term built in the reduced $\mathbb{R}^{n-m}$ modal space rather than in the full $\mathbb{R}^n$ geometrical space has been proposed in reference [9]. Unfortunately, since the number of modes retained in the analysis, m, is generally much less than the number of degrees of freedom (DoFs), n, the practical impact of this improvement tends to vanish for very large structural systems. Di Paola and Failla [9] also provides a rigorous criterion for the convergence of modal correction, that is: the highest natural frequency of the retained modes of vibration, $\widetilde{\omega}_m$, must be larger than the maximum frequency of the input. Indeed, if the opposite happens, the resonant contributions of some of the higher modes may become important, if not predominant, and so these modes should be retained in the dynamic analysis.

*Corresponding author
Email address: a.palmeri@lboro.ac.uk, dynamics.structures@gmail.com (Alessandro Palmeri)

Strategies of modal corrections specifically tailored to continuous structures, e.g. slender Euler-Bernoulli beams under fixed and moving loads, have been also proposed in a handful of articles [10–14] by extending the methods discussed above for discrete structures, and thus they enjoy the same advantages and suffers from the same disadvantages.

The availability of effective modal correction techniques is even more important in presence of random dynamic loadings. Indeed, methods to evaluate the response statistics in the probabilistic framework can be very time consuming for large systems, and hence any strategy capable to reduce the size of the problem without compromising the accuracy are very valuable. Nonetheless, little attention has been paid over the years to this topic. Direct extensions of FDM [15] and IDCM [16] for structures subjected to random excitations are available in the literature, but their applicability in practical situations is limited, since they require either a finite value for the variance of the dynamic input or an excessive computational effort, respectively. More recently, a proper stochastic MAM (SMAM) correction has been proposed by Cacciola et al. [17], which operates directly onto the differential equations governing first- and second-order statistics of the structural response. Although very interesting from a theoretical point of view, the SMAM correction needs the inversion of a matrix of size $(2n)^2$, n being the number of structural DoFs. The authors suggest $(2n)^2$ recursive applications of the Shermon-Morrison formula [18], to mitigate the computational effort, which may be time-consuming for very large structural systems. Moreover, the extension of the SMAM to continuous structures does not appear to be straightforward.

Aimed at overcoming these limitations, a novel modal correction method is proposed in this paper. The new technique, termed dynamic MAM (DyMAM), is initially formulated under the assumption that loads are deterministic. It is shown that the DyMAM corrective terms involve a number of additional dummy oscillators equal to the number of dynamic loads, which is generally much less than the number of the DoFs of the structure. This makes the procedure particularly appealing from a computational point of view. It is also shown that, similarly to the classical MAM, the proposed DyMAM works for both discrete and continuous structural systems. In a second stage, the proposed approach is extended to cope with random dynamic loads, therefore demonstrating the versatility of the proposed strategy of modal correction. Numerical examples prove accuracy and computational efficiency of DyMAM corrections in both deterministic and random settings.

2. Modal Acceleration Method (MAM)

Let us consider a discrete structure with n DoFs (degrees of freedom) subjected to ℓ dynamic loadings. Within the linear range, the equations of motion can be posed in the form:

$$\mathbf{M} \cdot \ddot{\mathbf{u}}(t) + \mathbf{C} \cdot \dot{\mathbf{u}}(t) + \mathbf{K} \cdot \mathbf{u}(t) = \mathbf{F} \cdot \mathbf{w}(t), \tag{1}$$

where $\mathbf{u}(t) = \{u_1(t) \dots u_n(t)\}^{\mathrm{T}}$ and $\mathbf{w}(t) = \{w_1(t) \dots w_\ell(t)\}^{\mathrm{T}}$ are the arrays listing DoFs of the structure and dynamic loadings, the superscript T being the transpose operator; $\mathbf{M}$, $\mathbf{C}$ and $\mathbf{K}$ are the n-dimensional matrices of mass, viscous damping and elastic stiffness; the over-dot denotes the time derivative; and where $\mathbf{F} = [\,\mathbf{f}_1 \dots \mathbf{f}_\ell\,]$ is the $n \times \ell$ tall matrix collecting the n-dimensional influence vectors for the ℓ dynamic loadings. In earthquake engineering, ℓ is the number of components of the ground acceleration, while in wind engineering ℓ may be the number of statistically independent components of the field of wind velocity.

In order to reduce the size of the problem in presence of large structural systems, the equations of motion are usually projected onto the modal space, which in turn is defined by the real-valued eigenproblem:

$$\widetilde{\omega}_j^2 \, \mathbf{M} \cdot \widetilde{\boldsymbol{\phi}}_j = \mathbf{K} \cdot \widetilde{\boldsymbol{\phi}}_j, \tag{2}$$

with the ortho-normalisation condition $\widetilde{\boldsymbol{\phi}}_i^{\mathrm{T}} \cdot \mathbf{M} \cdot \widetilde{\boldsymbol{\phi}}_j = \delta_{i,j}$, the symbol $\delta_{i,j}$ being the Kronecker's delta, equal to 1 when $i = j$, 0 otherwise.

In most civil engineering applications, the number m of vibrational modes retained in the analysis is much less than n. In earthquake engineering, for instance, building codes simply require that the modal mass participating in the seismic motion of the structure exceeds a given threshold, e.g. 90% as in the Eurocode 8 [1]. For an angle of attach α of the ground shaking, this condition can be expressed in the form:

$$\sum_{j=1}^{m} p_j^2(\alpha) \geq 0.90 M_{\mathrm{tot}}, \tag{3}$$

where M_{tot} is the total mass of the structure, while $p_j^2(\alpha)$ is the coefficient of modal participation for the j-th mode, given by:

$$p_j(\alpha) = \widetilde{\boldsymbol{\phi}}_j^{\mathrm{T}} \cdot \mathbf{f}_k, \tag{4}$$

in which $\mathbf{f}_k$ is the influence vector for the ground acceleration $w_k(t)$ along a generic angle of attack α.

If the structure is classically damped, i.e. if the well known Caughey-O'Kelly condition is met [19], the equations of motion turn out to be decoupled in the modal space:

$$\ddot{q}_j(t) + 2\,\widetilde{\zeta}_j\,\widetilde{\omega}_j\,\dot{q}_j(t) + \widetilde{\omega}_j^2\,q_j(t) = \widetilde{\boldsymbol{\phi}}_j^{\mathrm{T}} \cdot \sum_{k=1}^{\ell} \mathbf{f}_k\, w_k(t), \tag{5}$$

where $\widetilde{\zeta}_j$ is the viscous damping ratio in the j-th mode of vibration.

Once the modal equations of motion are solved, the dynamic response in terms of structural DoFs can be obtained by projecting back the modal responses onto the geometrical space of the system:

$$\widetilde{\mathbf{u}}(t) = \sum_{j=1}^{m} \widetilde{\boldsymbol{\phi}}_j\, q_j(t) = \mathbf{u}_{\mathrm{MDM}}(t), \tag{6}$$

where the over-tilde means that the structural responses so computed are approximate because the higher $(n - m)$ modes of vibration are neglected, while the subscript MDM stands for the classical modal displacement method.

Even though accurate in terms of absolute displacements of the structure, the effects of the modal truncation in the MDM can be quite large on relative displacements and internal forces. Indeed, once the higher modes are truncated, the dynamic system appears in the analyses fictiously more stiff, which may result in significantly under- or over- estimating the actual dynamic response.

In order to include in the analysis the additional flexibility arising from the neglected modes of vibration, the MAM (modal acceleration method) has been proposed [2, 3]. The correction formula can be expressed as:

$$\mathbf{u}_{\mathrm{MAM}}(t) = \widetilde{\mathbf{u}}(t) + \Delta\mathbf{u}_{\mathrm{MAM}}(t), \tag{7}$$

where:

$$\Delta\mathbf{u}_{\mathrm{MAM}}(t) = \overline{\mathbf{A}} \cdot \sum_{k=1}^{\ell} \mathbf{f}_k \, w_k(t), \tag{8}$$

in which the reduced flexibility matrix of the structure is given by:

$$\overline{\mathbf{A}} = \mathbf{K}^{-1} - \sum_{j=1}^{m} \frac{1}{\omega_j^2} \, \widetilde{\boldsymbol{\phi}}_j \cdot \widetilde{\boldsymbol{\phi}}_j^{\mathrm{T}} \, . \tag{9}$$

The MAM is able to correct the dynamic response in the low-frequency range, but introduces at the same time an error in the high-frequency range. This can be easily shown by considering the Fourier's transform of both sides of equation (7):

$$\begin{aligned} \mathrm{FT}\langle \mathbf{u}_{\mathrm{MAM}}(t) \rangle =& \mathrm{FT}\langle \widetilde{\mathbf{u}}(t) \rangle + \mathrm{FT}\langle \Delta\mathbf{u}_{\mathrm{MAM}}(t) \rangle \\ =& \mathbf{H}_{\mathrm{MAM}}(\omega) \cdot \sum_{k=1}^{\ell} \mathbf{f}_k \, \mathrm{FT}\langle w_k(t) \rangle, \end{aligned} \tag{10}$$

where $\mathrm{FT}\langle\cdot\rangle$ stands for the Fourier's transform operator, while $\mathbf{H}_{\mathrm{MAM}}(\omega)$ is the $n \times n$ matrix collecting the complex-valued FRFs (frequency response functions) obtained with m modes of vibration and MAM correction:

$$\mathbf{H}_{\mathrm{MAM}}(\omega) = \sum_{j=1}^{m} \widetilde{\boldsymbol{\phi}}_j \cdot \widetilde{\boldsymbol{\phi}}_j^{\mathrm{T}} \, \widetilde{H}_j(\omega) + \overline{\mathbf{A}}, \tag{11}$$

$\widetilde{\mathrm{H}}_j(\omega)$ being the FRF for the j-th mode of vibration:

$$\widetilde{H}_j(\omega) = \frac{1}{\widetilde{\omega}_j^2 - \omega^2 + 2\,\mathrm{i}\,\widetilde{\zeta}_j \, \widetilde{\omega}_j \, \omega}, \tag{12}$$

in which $\mathrm{i} = \sqrt{-1}$ is the imaginary unit.

The approximate FRF matrix $\mathbf{H}_{\mathrm{MAM}}(\omega)$ converges to the exact one $\mathbf{H}(\omega)$ when the frequency of vibration goes to zero. That is:

$$\mathbf{H}(\omega) = \left[\mathbf{K} - \omega^2 \mathbf{M} + \mathrm{i}\omega \mathbf{C} \right]^{-1}, \tag{13}$$

which at $\omega = 0$ reduces to:

$$\mathbf{H}(0) = \mathbf{K}^{-1} = \mathbf{H}_{\mathrm{MAM}}(0). \tag{14}$$

On the contrary, when ω goes to infinity the approximate FRF matrix of the MAM converges to the reduced flexibility matrix $\overline{\mathbf{A}}$, while the exact one approaches a null matrix:

$$\lim_{\omega \to \infty} \mathbf{H}(\omega) = \mathbf{O}_{n \times n} \neq \lim_{\omega \to \infty} \mathbf{H}_{\mathrm{MAM}}(\omega) = \overline{\mathbf{A}}, \tag{15}$$

in which $\mathbf{O}_{r \times s}$ is a zero matrix with r rows and s columns. Since $\overline{\mathbf{A}}$ is the correction term in the right-hand side of equation (11), it follows that the more the MAM improves the solution at low frequencies, the larger is the inaccuracy introduced at high frequencies .

3. Dynamic MAM (DyMAM)

In the previous section, it has been shown that the classical MAM is unable to correct the dynamic response in the low-frequency range without introducing a systematic error in the high-frequency range. Aim of this section is to formulate a novel correction strategy which keeps the improvement of the MAM for low frequencies without affecting high frequencies. It is anticipated that the proposed modal correction method enjoys improved performances at low frequencies too. This goal can be achieved by modifying the dynamic loading in the right-hand side of equation (8):

$$\Delta\mathbf{u}_{\mathrm{DyMAM}}(t) = \overline{\mathbf{A}} \cdot \sum_{k=1}^{\ell} \mathbf{f}_k \, \theta_k(t), \tag{16}$$

in which the subscript DyMAM stands for dynamic MAM, since $\theta_k(t)$ is the k-th dynamic loading $w_k(t)$ properly filtered through an elementary dynamic system, namely a single-DoF oscillator with undamped circular frequency of vibration $\overline{\omega}_k$ and viscous damping ratio $\overline{\zeta}_k$. That is, the novel variable $\theta_k(t)$ is ruled by a second-order linear differential equation formally similar to the equation of motion of a single-DoF oscillator forced by the dynamic loading $w_k(t)$:

$$\ddot{\theta}_k(t) + 2\,\overline{\zeta}_k \, \overline{\omega}_k \, \dot{\theta}_k(t) + \overline{\omega}_k^2 \, \theta_k(t) = \overline{\omega}_k^2 w_k(t). \tag{17}$$

The reason for filtering the dynamic input $w_k(t)$ is to avoid undesirable high-frequency contributions arising from the modal correction term. Amongst possible filters for the dynamic excitation $w_k(t)$, a single-DoF has been chosen herein because it allows handling the corrective output $\theta_k(t)$ similarly to the j-th modal response $q_j(t)$, e.g. standard strategies of structural dynamics can be applied. As a side advantage, practitioner structural engineers do not require further knowledge to understand the effects of such filtering. This choice enables also a physical justification of the DyMAM correction. The idea is indeed to attach the flexibility of higher modes of vibration to the corresponding residual inertia, therefore having a single-DoF equipped with stiffness and mass which are not taken into account with the first m modes in the MDM. Accordingly, the circular frequency $\overline{\omega}_k$ of the filter associated with the k-th dynamic load can be evaluated by resorting to the concept of Rayleigh's quotient [20], which for a discrete structural system takes the form:

$$\overline{\omega}_k = \sqrt{\frac{\overline{\mathbf{u}}_k^{\mathrm{T}} \cdot \left[\mathbf{K} - \mathbf{M} \cdot \widetilde{\boldsymbol{\Phi}} \cdot \widetilde{\boldsymbol{\Omega}}^2 \cdot \widetilde{\boldsymbol{\Phi}}^{\mathrm{T}} \cdot \mathbf{M} \right] \cdot \overline{\mathbf{u}}_k}{\overline{\mathbf{u}}_k^{\mathrm{T}} \cdot \left[\mathbf{M} - \mathbf{M} \cdot \widetilde{\boldsymbol{\Phi}} \cdot \widetilde{\boldsymbol{\Phi}}^{\mathrm{T}} \cdot \mathbf{M} \right] \cdot \overline{\mathbf{u}}_k}}, \tag{18}$$

where $\overline{\mathbf{u}}_k = \mathbf{K}^{-1} \cdot \mathbf{f}_k$ represents the deformed shape under the k-th influence vector $\mathbf{f}_k$; $\widetilde{\mathbf{\Omega}}$ is the m-dimensional spectral matrix of the structure, listing the first m undamped circular frequencies:

$$\widetilde{\mathbf{\Omega}} = \text{diag}\left[\, \widetilde{\omega}_1 \dots \widetilde{\omega}_m \,\right], \tag{19}$$

the diag[·] operator returning a diagonal matrix from the elements within square brackets, while the matrices at numerator and denominator in equation (18) are the residual matrices of stiffness and mass, respectively, which in turn are obtained by removing from $\mathbf{K}$ and $\mathbf{M}$ the contributions of the first m modes of vibration.

After simple algebra, equation (18) can be posed in the alternative form:

$$\overline{\omega}_k = \sqrt{\frac{\overline{\mathbf{u}}_k^{\mathrm{T}} \cdot \mathbf{K} \cdot \overline{\mathbf{u}}_k - \overline{\mathbf{q}}_k^{\mathrm{T}} \cdot \widetilde{\mathbf{\Omega}}^2 \cdot \overline{\mathbf{q}}_k}{\overline{\mathbf{u}}_k^{\mathrm{T}} \cdot \mathbf{M} \cdot \overline{\mathbf{u}}_k - \overline{\mathbf{q}}_k^{\mathrm{T}} \cdot \overline{\mathbf{q}}_k}}, \tag{20}$$

where $\overline{\mathbf{q}}_k = \widetilde{\mathbf{\Phi}}^{\mathrm{T}} \cdot \mathbf{M} \cdot \mathbf{u_k}$ is the projection of $\overline{\mathbf{u}}_k$ onto the reduced modal space, being:

$$\widetilde{\mathbf{\Phi}} = [\widetilde{\boldsymbol{\phi}}_1 \dots \widetilde{\boldsymbol{\phi}}_m] \tag{21}$$

the $n \times m$ tall matrix collecting the first m modal shapes of the structure.

Numerator and denominator in equation (20) are respectively proportional to residual potential energy and residual kinetic energy of the structure vibrating with the deformed shape $\overline{\mathbf{u}}_k$ once the contributions of the first m modes, vibrating according to the array $\overline{\mathbf{q}}_k$, have been removed.

The value of the viscous damping ratio $\overline{\zeta}_k$ for the k-th filter can be evaluated by using the Rayleigh's model of viscous damping [20]:

$$\overline{\zeta}_k = \frac{1}{2\,\overline{\omega}_k} \cdot \alpha_{\mathrm{M}} + \frac{\overline{\omega}_k}{2} \alpha_{\mathrm{K}}^{-1}, \tag{22}$$

where the coefficients α_{M} and α_{K}, with the same dimensions as a circular frequency, are given by:

$$\alpha_{\mathrm{M}} = \frac{2}{\widetilde{\omega}_m^2 - \widetilde{\omega}_1^2}\, \widetilde{\omega}_1 \widetilde{\omega}_m \left(\widetilde{\omega}_m \widetilde{\zeta}_1 - \widetilde{\omega}_1 \widetilde{\zeta}_m \right); \tag{23a}$$

$$\alpha_{\mathrm{K}} = \frac{\widetilde{\omega}_m^2 - \widetilde{\omega}_1^2}{2}\, \frac{1}{\widetilde{\omega}_m \widetilde{\zeta}_m - \widetilde{\omega}_1 \widetilde{\zeta}_1} \tag{23b}$$

while the viscous damping matrix of the whole structure can be expressed as:

$$\begin{aligned} \mathbf{C} = {} & \mathbf{M} \cdot \widetilde{\mathbf{\Phi}} \cdot \widetilde{\mathbf{\Xi}} \cdot \widetilde{\mathbf{\Phi}}^{\mathrm{T}} \cdot \mathbf{M} \\ & + \alpha_{\mathrm{M}} \left[\mathbf{M} - \mathbf{M} \cdot \widetilde{\mathbf{\Phi}} \cdot \widetilde{\mathbf{\Phi}}^{\mathrm{T}} \cdot \mathbf{M} \right] \\ & + \alpha_{\mathrm{K}} \left[\mathbf{K} - \mathbf{M} \cdot \widetilde{\mathbf{\Phi}} \cdot \mathbf{\Omega}^2 \cdot \widetilde{\mathbf{\Phi}}^{\mathrm{T}} \cdot \mathbf{M} \right], \end{aligned} \tag{24}$$

in which $\widetilde{\mathbf{\Xi}}$ is the m-dimensional matrix of modal damping:

$$\widetilde{\mathbf{\Xi}} = 2\ \text{diag}\left[\, \widetilde{\zeta}_1 \dots \widetilde{\zeta}_m \,\right] \cdot \widetilde{\mathbf{\Omega}}\,. \tag{25}$$

Equation (24) shows that, according to the DyMAM correction approach, the viscous damping matrix can be consistently built as superposition of three contributions, namely: i) viscous damping due to the m modes of vibration retained in the analysis; ii) dissipation term proportional to the residual mass; iii) dissipation term proportional to the residual stiffness. The matrix $\mathbf{C}$ so obtained will be used in the numerical applications for validation purposes.

Once circular frequencies and viscous damping ratios of the auxiliary dummy oscillators have been defined, the equations ruling the DyMAM take the matrix form:

$$\ddot{\mathbf{q}}(t) + \widetilde{\mathbf{\Xi}} \cdot \dot{\mathbf{q}}(t) + \widetilde{\mathbf{\Omega}}^2 \cdot \mathbf{q}(t) = \widetilde{\mathbf{\Phi}}^{\mathrm{T}} \cdot \mathbf{F} \cdot \mathbf{w}(t); \tag{26a}$$

$$\ddot{\boldsymbol{\theta}}(t) + \overline{\mathbf{\Xi}} \cdot \dot{\boldsymbol{\theta}}(t) + \overline{\mathbf{\Omega}}^2 \cdot \boldsymbol{\theta}(t) = \overline{\mathbf{\Omega}}^2 \cdot \mathbf{w}(t), \tag{26b}$$

where the arrays $\mathbf{q}(t) = \{q_1(t) \dots q_m(t)\}^{\mathrm{T}}$ and $\boldsymbol{\theta}(t) = \{\theta_1(t) \dots \theta_\ell(t)\}^{\mathrm{T}}$ collect m modal coordinates and ℓ filtered loadings, respectively, while $\overline{\mathbf{\Omega}}$ and $\overline{\mathbf{\Xi}}$ are spectral and damping matrices for the novel array $\boldsymbol{\theta}(t)$:

$$\overline{\mathbf{\Omega}} = \text{diag}\left[\, \overline{\omega}_1 \dots \overline{\omega}_\ell \,\right]; \tag{27a}$$

$$\overline{\mathbf{\Xi}} = 2\ \text{diag}\left[\, \overline{\zeta}_1 \dots \overline{\zeta}_\ell \,\right] \cdot \overline{\mathbf{\Omega}}\,. \tag{27b}$$

Equations (26a) and (26b) can be solved independently, and their responses can be superimposed in order to get the corrected time histories of the structural DoFs:

$$\begin{aligned} \mathbf{u}_{\mathrm{DyMAM}}(t) = {} & \widetilde{\mathbf{u}}(t) + \Delta\mathbf{u}_{\mathrm{DyMAM}}(t) \\ = {} & \widetilde{\mathbf{\Phi}} \cdot \mathbf{q}(t) + \overline{\mathbf{A}} \cdot \mathbf{F} \cdot \boldsymbol{\theta}(t). \end{aligned} \tag{28}$$

By taking the Fourier's transform of equation (28), after some algebra, one obtains the approximate FRF matrix consistent with the DyMAM correction:

$$\begin{aligned} \mathrm{FT}\langle \mathbf{u}_{\mathrm{DyMAM}}(t) \rangle = {} & \widetilde{\mathbf{\Phi}} \cdot \mathrm{FT}\langle \mathbf{q}(t) \rangle + \overline{\mathbf{A}} \cdot \mathbf{F} \cdot \mathrm{FT}\langle \boldsymbol{\theta}(t) \rangle \\ = {} & \mathbf{H}_{\mathrm{DyMAM}}(\omega) \cdot \mathbf{F} \cdot \mathrm{FT}\langle \mathbf{w}(t) \rangle, \end{aligned} \tag{29}$$

where

$$\mathbf{H}_{\mathrm{DyMAM}}(\omega) = \widetilde{\mathbf{\Phi}} \cdot \widetilde{\mathbf{H}}(\omega) \cdot \mathbf{\Phi}^{\mathrm{T}} + \overline{\mathbf{A}} \cdot \mathbf{F} \cdot \overline{\mathbf{H}}(\omega), \tag{30}$$

in which $\widetilde{\mathbf{H}}(\omega)$ and $\overline{\mathbf{H}}(\omega)$ are the matrices collecting the FRFs for the first m modes of vibration and the ℓ dummy oscillators, respectively:

$$\widetilde{\mathbf{H}}(\omega) = \text{diag}\left[\, \widetilde{H}_1(\omega) \dots \widetilde{H}_m(\omega) \,\right]; \tag{31a}$$

$$\overline{\mathbf{H}}(\omega) = \text{diag}\left[\, \overline{H}_1(\omega) \dots \overline{H}_\ell(\omega) \,\right], \tag{31b}$$

whose k-th elements are given by equations (12) for the former matrix and by:

$$\overline{H}_k(\omega) = \frac{\overline{\omega}_k^2}{\overline{\omega}_k^2 - \omega^2 + 2\,\mathrm{i}\,\overline{\zeta}_k\,\omega_k}, \tag{32}$$

for the latter matrix, respectively.

Importantly, both the limiting conditions at $\omega = 0$ and when ω goes to infinity are satisfied by the novel FRF matrix:

$$\mathbf{H}_{\mathrm{DyMAM}}(0) = \mathbf{K}^{-1}; \quad \lim_{\omega \to +\infty} \mathbf{H}_{\mathrm{DyMAM}}(\omega) = \mathbf{O}_{n \times n}. \tag{33}$$

3.1. Continuous structure

The proposed DyMAM correction lends itself to be extended to cope with continuous structures under dynamic loadings. Without lack of generality, let us consider a slender beam of length L subjected to ℓ time-varying concentrated forces. The problem in hand is ruled by the partial differential equation:

$$\mu(z)\,\frac{\partial^2}{\partial t^2}u(z,t)+\frac{\partial^2}{\partial z^2}\left(\kappa(z)\frac{\partial^2}{\partial z^2}u(z,t)\right)+D(z,t)=\sum_{k=1}^{\ell}\delta\left(z-\overline{z}_k\right)\,w_k(t), \tag{34}$$

where $\mu(z)$ and $\kappa(z)$ are mass per unit length and flexural stiffness of the beam; $u(z,t)$ is the time-dependent field of transverse displacements, while $D(z,t)$ is the damping force per unit length, which can be assumed to be of viscous nature; the pair $\{\overline{z}_k, w_k(t)\}$ defines position and intensity of the k-th load, while $\delta(\cdot)$ is the Dirac's delta function, which in turn is defined as the derivative of the Heaviside's unit step function $\mathrm{U}(\cdot)$:

$$\delta(z)=\frac{\mathrm{d}}{\mathrm{d}z}\mathrm{U}(z);\quad \mathrm{U}(z)=\begin{cases}0, & z<0,\\ \frac{1}{2}, & z=0,\\ 1, & z>0.\end{cases} \tag{35}$$

An approximate solution of equation (34) can be derived by applying the classical modal analysis. Accordingly, the field of transverse displacements is expressed as superposition of the first m modal shapes of the beam (analogous to equation (6)):

$$\widetilde{u}(z,t)=\sum_{j=1}^{m}\widetilde{\phi}_j(z)\,q_j(t)=u_{\mathrm{MDM}}(z,t), \tag{36}$$

where $q_j(t)$ is the j-th modal coordinate and $\widetilde{\phi}_j(z)$ is the associated modal shape, to be evaluated along with the j-th modal circular frequency $\widetilde{\omega}_j$ as solution of the eigenproblem (corresponding to equation (2)):

$$\widetilde{\omega}_j^2\,\mu(z)\,\widetilde{\phi}_j(z)=\frac{\mathrm{d}^2}{\mathrm{d}z^2}\left(\kappa(z)\,\frac{\mathrm{d}^2}{\mathrm{d}z^2}\,\widetilde{\phi}_j(z)\right), \tag{37}$$

coupled with ortho-normalisation condition:

$$\int_0^L\mu(z)\,\widetilde{\phi}_i(z)\,\widetilde{\phi}_j(z)\,\mathrm{d}z=\delta_{i,j}, \tag{38}$$

and pertinent boundary conditions.

(39)

Substituting equation (36) into equation (34), premultiplying both sides by $\widetilde{\phi}_j(z)$, and integrating from 0 to L with respect to z, one obtains (analogous to equation (5)):

$$\ddot{q}_j(t)+2\,\widetilde{\zeta}_j\,\widetilde{\omega}_j\,\dot{q}(t)+\widetilde{\omega}_j^2\,q_j(t)=\sum_{k=1}^{\ell}\widetilde{\phi}_j(\overline{z}_k)\,w_k(t). \tag{40}$$

The DyMAM correction of the beam's dynamic response can be expressed as (similar to equation (28)):

$$\begin{aligned}u_{\mathrm{DyMAM}}(z,t)&=\tilde{u}(z,t)+\Delta u_{\mathrm{DyMAM}}(z,t)\\&=\tilde{\boldsymbol{\phi}}^{\mathrm{T}}(z)\cdot\mathbf{q}(t)+\overline{\mathbf{g}}^{\mathrm{T}}(z)\cdot\boldsymbol{\theta}(t),\end{aligned} \tag{41}$$

where $\widetilde{\boldsymbol{\phi}}(z)=\left\{\widetilde{\phi}_1(z)\ldots\widetilde{\phi}_m(z)\right\}^{\mathrm{T}}$ and $\mathbf{q}(t)=\{q_1(t)\ldots q_m(t)\}^{\mathrm{T}}$ are the m-dimensional arrays listing modal shapes and modal coordinates of the beam; $\boldsymbol{\theta}(t)=\{\theta_1(t)\ldots\theta_\ell(t)\}^{\mathrm{T}}$ is the array of ℓ filtered dynamic loadings, which are distinctive of the proposed approach, while $\overline{\mathbf{g}}(z)=\left\{\overline{\mathrm{G}}(z,\overline{z}_1)\ldots\overline{\mathrm{G}}(z,\overline{z}_\ell)\right\}^{\mathrm{T}}$ is the time-dependent array collecting the reduced Green's function of the beam evaluated at the position of the ℓ dynamic loadings. It is worth emphasizing that the reduced Green's function $\overline{\mathrm{G}}(z,\overline{z})$ for a continuous structure plays the same role as the reduced flexibility matrix $\overline{\mathbf{A}}$ for a discrete structure. Indeed, the definition of the function $\overline{\mathrm{G}}(z,\overline{z})$ is similar to that one of the matrix $\overline{\mathrm{A}}$ (see equation (9)):

$$\overline{\mathrm{G}}(z,\overline{z})=\mathrm{G}(z,\overline{z})-\sum_{j=1}^{m}\frac{1}{\omega_j^2}\,\widetilde{\phi}_j(z)\,\widetilde{\phi}_j(\overline{z}), \tag{42}$$

in which $\mathrm{G}(z,\overline{z})$ is the actual Green's function of the beam, satisfying the static bending equation:

$$\frac{\mathrm{d}^2}{\mathrm{d}z^2}\left(\kappa(z)\,\frac{\mathrm{d}^2}{\mathrm{d}z^2}\mathrm{G}(z,\overline{z})\right)=\delta(z-\overline{z}), \tag{43}$$

with the appropriate boundary conditions.

(44)

Also the evolution in time of arrays $\mathbf{q}(t)$ and $\boldsymbol{\theta}(t)$ appearing in equation (41) for continuous structures is ruled similarly to the analogous arrays for discrete structures (see equations (26)):

$$\ddot{\mathbf{q}}(t)+\widetilde{\boldsymbol{\Xi}}\cdot\dot{\mathbf{q}}(t)+\widetilde{\boldsymbol{\Omega}}^2\cdot\mathbf{q}(t)=\widetilde{\mathbf{F}}\cdot\mathbf{w}(t); \tag{45a}$$

$$\ddot{\boldsymbol{\theta}}(t)+\overline{\boldsymbol{\Xi}}\cdot\dot{\boldsymbol{\theta}}(t)+\overline{\boldsymbol{\Omega}}^2\cdot\boldsymbol{\theta}(t)=\overline{\boldsymbol{\Omega}}^2\cdot\mathbf{w}(t), \tag{45b}$$

where the rectangular matrix $\widetilde{\mathbf{F}}$ collects the modal forcing coefficients of equation (40):

$$\widetilde{\mathbf{F}}=\begin{bmatrix}\widetilde{\phi}_1(\overline{z}_1) & \cdots & \widetilde{\phi}_1(\overline{z}_\ell)\\ \vdots & \ddots & \vdots\\ \widetilde{\phi}_m(\overline{z}_1) & \cdots & \widetilde{\phi}_m(\overline{z}_\ell)\end{bmatrix}, \tag{46}$$

while the other matrices take the very same expressions as for discrete structures (see equations (19), (25) and (27)):

$$\widetilde{\boldsymbol{\Omega}}=\mathrm{diag}\left[\,\omega_1\ldots\omega_n\,\right];\quad \widetilde{\boldsymbol{\Xi}}=2\,\mathrm{diag}\left[\,\zeta_1\ldots\zeta_m\,\right]\cdot\widetilde{\boldsymbol{\Omega}}; \tag{47a}$$

$$\overline{\boldsymbol{\Omega}}=\mathrm{diag}\left[\,\overline{\omega}_1\ldots\overline{\omega}_\ell\,\right];\quad \overline{\boldsymbol{\Xi}}=2\,\mathrm{diag}\left[\,\overline{\zeta}_1\ldots\overline{\zeta}_\ell\,\right]\cdot\overline{\boldsymbol{\Omega}}. \tag{47b}$$

The k-th circular frequency appearing in the first of equations (47b) can be evaluated by rewriting equation (20) for continuous rather than discrete structures:

$$\overline{\omega}_k=\sqrt{\frac{\int_0^L\kappa(z)\left[\frac{\mathrm{d}^2}{\mathrm{d}z^2}\,\mathrm{G}(z,\overline{z}_k)\right]^2\mathrm{d}z-\overline{\mathbf{q}}_k^{\mathrm{T}}\cdot\widetilde{\boldsymbol{\Omega}}^2\cdot\overline{\mathbf{q}}_k}{\int_0^L\mu(z)\,\mathrm{G}(z,\overline{z}_k)^2\,\mathrm{d}z-\overline{\mathbf{q}}_k^{\mathrm{T}}\cdot\overline{\mathbf{q}}_k}}, \tag{48}$$

where the array $\overline{\mathbf{q}}_k$ describes in the m-dimensional modal space the deformed shape of the slender beam under investigation induced by a unit point load at $z = \overline{z}_k$:

$$\overline{\mathbf{q}}_k = \int_0^L \mu(z)\,\boldsymbol{\phi}(z)\,\mathrm{G}(z,\overline{z}_k)\,\mathrm{d}z. \tag{49}$$

The k-th viscous damping ratio in the second of equations (47b) can be determined through equations (22) and (23), which are valid for both discrete and continuous systems.

4. Numerical solution for deterministic DyMAM correction

In the previous section, the differential equations ruling the dynamic response of discrete (equations (26)) and continuous (equations (45)) structures with the proposed DyMAM correction have been derived. Aim of this section is to present integral and incremental solutions for these equations.

To do so, let us introduce the array of traditional state variables for the structural system in the modal space, $\mathbf{x}(t) = \left\{ \mathbf{q}(t)^{\mathrm{T}} \;\vdots\; \dot{\mathbf{q}}(t)^{\mathrm{T}} \right\}^{\mathrm{T}}$, collecting modal displacements and modal velocities, along with the novel array, $\mathbf{y}(t) = \left\{ \boldsymbol{\theta}(t)^{\mathrm{T}} \;\vdots\; \dot{\boldsymbol{\theta}}(t)^{\mathrm{T}} \right\}^{\mathrm{T}}$, listing the state variables associated with the filtered dynamic loadings.

The evolution in time of the state arrays $\mathbf{x}(t)$ and $\mathbf{y}(t)$ is ruled by:

$$\dot{\mathbf{x}}(t) = \widetilde{\mathbf{D}} \cdot \mathbf{x}(t) + \widetilde{\mathbf{V}} \cdot \mathbf{w}(t); \tag{50a}$$

$$\dot{\mathbf{y}}(t) = \overline{\mathbf{D}} \cdot \mathbf{y}(t) + \overline{\mathbf{V}} \cdot \mathbf{w}(t), \tag{50b}$$

where:

$$\widetilde{\mathbf{D}} = \left[\begin{array}{c:c} \mathbf{O}_{m\times m} & \mathbf{I}_m \\ \hdashline -\widetilde{\boldsymbol{\Xi}} & -\widetilde{\boldsymbol{\Omega}}^2 \end{array}\right]; \quad \overline{\mathbf{D}} = \left[\begin{array}{c:c} \mathbf{O}_{\ell\times\ell} & \mathbf{I}_\ell \\ \hdashline -\overline{\boldsymbol{\Xi}} & -\overline{\boldsymbol{\Omega}}^2 \end{array}\right]; \quad \overline{\mathbf{V}} = \left[\begin{array}{c} \mathbf{O}_{\ell\times\ell} \\ \hdashline \overline{\boldsymbol{\Omega}}^2 \end{array}\right], \tag{51}$$

$\mathbf{I}_s$ being the identity matrix of size s, while the rectangular matrix $\widetilde{\mathbf{V}}$ takes different expressions for discrete structures (see equation (26a)):

$$\widetilde{\mathbf{V}} = \left[\begin{array}{c} \mathbf{O}_{m\times\ell} \\ \hdashline \widetilde{\boldsymbol{\Phi}}^{\mathrm{T}} \cdot \mathbf{F} \end{array}\right], \tag{52a}$$

and continuous ones (see equation (45a)):

$$\widetilde{\mathbf{V}} = \left[\begin{array}{c} \mathbf{O}_{m\times\ell} \\ \hdashline \widetilde{\mathbf{F}} \end{array}\right]. \tag{52b}$$

The following time-domain single-step incremental solutions can be used in practice:

$$\begin{aligned} \mathbf{x}(t+\Delta t) = {} & \widetilde{\boldsymbol{\Theta}}(\Delta t)\cdot\mathbf{x}(t) + \widetilde{\boldsymbol{\Gamma}}'(\Delta t)\cdot\widetilde{\mathbf{V}}\cdot\mathbf{w}(t) \\ & + \widetilde{\boldsymbol{\Gamma}}''(\Delta t)\cdot\widetilde{\mathbf{V}}\cdot\mathbf{w}(t+\Delta t); \end{aligned} \tag{54a}$$

$$\begin{aligned} \mathbf{y}(t+\Delta t) = {} & \overline{\boldsymbol{\Theta}}(\Delta t)\cdot\mathbf{y}(t) + \overline{\boldsymbol{\Gamma}}'(\Delta t)\cdot\overline{\mathbf{V}}\cdot\mathbf{w}(t) \\ & + \overline{\boldsymbol{\Gamma}}''(\Delta t)\cdot\overline{\mathbf{V}}\cdot\mathbf{w}(t+\Delta t), \end{aligned} \tag{54b}$$

where Δt is the time step selected for the incremental solution, while the operators $\boldsymbol{\Theta}$ and $\boldsymbol{\Gamma}$ in the right-hand side of equations (54) are given in appendix A.

Once the state arrays $\mathbf{x}(t)$ and $\mathbf{y}(t)$ have been evaluated, and the sub-arrays $\mathbf{q}(t)$ and $\boldsymbol{\theta}(t)$ extracted, the structural response can be computed through equation (28) for a discrete system and equation (41) for a continuous one.

5. DyMAM correction with random loadings

In many engineering situations, dynamic loadings are not known in a deterministic sense, being properly described by random processes of given statistics. This is the case, for instance, of natural actions like ground shakings, wind gusts and ocean waves.

When the excitation is a random process, the dynamic response is random too, and hence the statistics of the response must be evaluated. For illustrative purpose, let us consider a discrete structural system subjected to one-dimensional (ℓ=1) seismic motion. Extension to multi-variate random excitations and/or continuous structures is straightforward. The mathematical derivation of the governing equations is offered herein for the simplest case of one-variate input and discrete structure to avoid heavier notations. For the problem in hand, equation (1) particularises as:

$$\mathbf{M}\cdot\ddot{\mathbf{u}}(t) + \mathbf{C}\cdot\dot{\mathbf{u}}(t) + \mathbf{K}\cdot\mathbf{u}(t) = \mathbf{f}\,w(t), \tag{55}$$

where $w(t)$ is the ground acceleration, which is modeled as a zero-mean Gaussian process, fully characterized by the auto-correlation function:

$$R_{ww}(t,\tau) = \mathrm{E}\langle\, w(t)\,w(\tau)\,\rangle, \tag{56}$$

where the symbol $\mathrm{E}\langle\cdot\rangle$ denotes the expectation operator.

Owing for the linearity of the structural system, one can easily prove that the dynamic response $\mathbf{u}(t)$ is a zero-mean Gaussian process, which in turn is fully characterized in a probabilistic sense by the n^2-dimensional array collecting auto- and cross-correlation functions:

$$\mathbf{r}_{\mathbf{uu}}(t,\tau) = \mathrm{E}\langle\, \mathbf{u}(t)\otimes\mathbf{u}(\tau)\,\rangle, \tag{57}$$

where $\otimes$ means Kronecker's product (see appendix B).

In many practical situations, however, engineering conclusions about serviceability and ultimate limit states can be drawn just considering variances and covariances of displacements and velocities of the system:

$$\boldsymbol{\sigma}_{\mathbf{u}}(t) = \mathrm{E}\langle\, \mathbf{u}(t)^{[2]}\,\rangle; \tag{58a}$$

$$\boldsymbol{\sigma}_{\dot{\mathbf{u}}}(t) = \mathrm{E}\langle\, \dot{\mathbf{u}}(t)^{[2]}\,\rangle, \tag{58b}$$

where the superscript [2] means Kronecker's square (see appendix B).

By taking into account equation (28), the DyMAM correction leads to the following expressions for the variance-covariance arrays of the structural response in terms of displacements and velocities:

$$\begin{aligned} \boldsymbol{\sigma}_{\mathbf{u},\mathrm{DyMAM}}(t) = {} & \widetilde{\boldsymbol{\Phi}}^{[2]}\cdot\mathrm{E}\langle\,\mathbf{q}(t)^{[2]}\,\rangle + \left\{\overline{\mathbf{A}}\cdot\mathbf{f}\right\}^{[2]}\mathrm{E}\langle\,\theta(t)^2\,\rangle \\ & + \left[\widetilde{\boldsymbol{\Phi}}\otimes\left\{\overline{\mathbf{A}}\cdot\mathbf{f}\right\} + \left\{\overline{\mathbf{A}}\cdot\mathbf{f}\right\}\otimes\widetilde{\boldsymbol{\Phi}}\right]\cdot\mathrm{E}\langle\,\mathbf{q}(t)\,\theta(t)\,\rangle; \end{aligned} \tag{59a}$$

$$\boldsymbol{\sigma}_{\ddot{\mathbf{u}},\mathrm{DyMAM}}(t) = \widetilde{\boldsymbol{\Phi}}^{[2]} \cdot \mathrm{E}\langle\, \dot{\mathbf{q}}(t)^{[2]} \,\rangle + \left\{\overline{\mathbf{A}} \cdot \mathbf{f}\right\}^{[2]} \mathrm{E}\langle\, \dot{\theta}(t)^2 \,\rangle \quad (59b)$$
$$+ \left[\widetilde{\boldsymbol{\Phi}} \otimes \left\{\overline{\mathbf{A}} \cdot \mathbf{f}\right\} + \left\{\overline{\mathbf{A}} \cdot \mathbf{f}\right\} \otimes \widetilde{\boldsymbol{\Phi}}\right] \cdot \mathrm{E}\langle\, \dot{\mathbf{q}}(t)\, \dot{\theta}(t) \,\rangle,$$

in which the properties of the Kronecker's algebra have been resorted to.

The statistics appearing in the right-hand side of equations (59) can be extracted from the variance-covariance arrays of traditional and additional state variables:

$$\mathrm{E}\langle\, \mathbf{x}(t)^{[2]} \,\rangle = \begin{Bmatrix} \mathrm{E}\langle\, q_1(t)^2 \,\rangle \\ \vdots \\ \mathrm{E}\langle\, q_m(t)^2 \,\rangle \end{Bmatrix}; \quad (60a)$$

$$\mathrm{E}\langle\, \mathbf{y}(t)^{[2]} \,\rangle = \begin{Bmatrix} \mathrm{E}\langle\, \theta(t)^2 \,\rangle \\ \vdots \\ \mathrm{E}\langle\, \dot{\theta}(t)^2 \,\rangle \end{Bmatrix}; \quad (60b)$$

$$\mathrm{E}\langle\, \mathbf{x}(t) \otimes \mathbf{y}(t) \,\rangle = \begin{Bmatrix} \mathrm{E}\langle\, q_1(t)\, \theta(t) \,\rangle \\ \vdots \\ \mathrm{E}\langle\, q_m(t)\, \dot{\theta}(t) \,\rangle \end{Bmatrix}, \quad (60c)$$

whose evolution in time is ruled by three decoupled sets of first-order linear differential equations:

$$\frac{\mathrm{d}}{\mathrm{d}t}\mathrm{E}\langle\, \mathbf{x}(t)^{[2]} \,\rangle = \mathrm{E}\langle\, \dot{\mathbf{x}}(t) \otimes \mathbf{x}(t) + \mathbf{x}(t) \otimes \dot{\mathbf{x}}(t) \,\rangle \quad (61a)$$
$$= \left[\widetilde{\mathbf{D}} \otimes \mathbf{I}_{2m} + \mathbf{I}_{2m} \otimes \widetilde{\mathbf{D}}\right] \cdot \mathrm{E}\langle\, \mathbf{x}(t)^{[2]} \,\rangle$$
$$+ \left[\widetilde{\mathbf{V}} \otimes \mathbf{I}_{2m} + \mathbf{I}_{2m} \otimes \widetilde{\mathbf{V}}\right] \cdot \mathrm{E}\langle\, \mathbf{x}(t)\, w(t) \,\rangle;$$

$$\frac{\mathrm{d}}{\mathrm{d}t}\mathrm{E}\langle\, \mathbf{y}(t)^{[2]} \,\rangle = \mathrm{E}\langle\, \dot{\mathbf{y}}(t) \otimes \mathbf{y}(t) + \mathbf{y}(t) \otimes \dot{\mathbf{y}}(t) \,\rangle \quad (61b)$$
$$= \left[\overline{\mathbf{D}} \otimes \mathbf{I}_{2\ell} + \mathbf{I}_{2\ell} \otimes \overline{\mathbf{D}}\right] \cdot \mathrm{E}\langle\, \mathbf{y}(t)^{[2]} \,\rangle$$
$$+ \left[\overline{\mathbf{V}} \otimes \mathbf{I}_{2\ell} + \mathbf{I}_{2\ell} \otimes \overline{\mathbf{V}}\right] \cdot \mathrm{E}\langle\, \mathbf{y}(t)\, w(t) \,\rangle;$$

$$\frac{\mathrm{d}}{\mathrm{d}t}\mathrm{E}\langle\, \mathbf{x}(t) \otimes \mathbf{y}(t) \,\rangle = \mathrm{E}\langle\, \dot{\mathbf{x}}(t) \otimes \mathbf{y}(t) + \mathbf{x}(t) \otimes \dot{\mathbf{y}}(t) \,\rangle \quad (61c)$$
$$= \left[\widetilde{\mathbf{D}} \otimes \mathbf{I}_{2\ell} + \mathbf{I}_{2m} \otimes \overline{\mathbf{D}}\right] \cdot \mathrm{E}\langle\, \mathbf{x}(t) \otimes \mathbf{y}(t) \,\rangle$$
$$+ \left[\widetilde{\mathbf{V}} \otimes \mathbf{I}_{2\ell}\right] \cdot \mathrm{E}\langle\, \mathbf{x}(t)\, w(t) \,\rangle$$
$$+ \left[\mathbf{I}_{2m} \otimes \overline{\mathbf{V}}\right] \cdot \mathrm{E}\langle\, \mathbf{y}(t)\, w(t) \,\rangle.$$

It can be proved that forcing terms in the right-hand side of equation (56) are given by the integral expressions:

$$\mathrm{E}\langle\, \mathbf{x}(t)\, w(t) \,\rangle = \int_0^t \widetilde{\boldsymbol{\Theta}}(t-\tau) \cdot \widetilde{\mathbf{V}}\, R_{ww}(t,\tau)\, \mathrm{d}\tau; \quad (62a)$$

$$\mathrm{E}\langle\, \mathbf{y}(t)\, w(t) \,\rangle = \int_0^t \overline{\boldsymbol{\Theta}}(t-\tau) \cdot \overline{\mathbf{V}}\, R_{ww}(t,\tau)\, \mathrm{d}\tau. \quad (62b)$$

The three steps listed below are then required:

1. Evaluation of the forcing term through equations (62);
2. Numerical integration of equations (61), which give the evolution in time of the second-order statistics of modal (classical) and loading (additional) state variables;

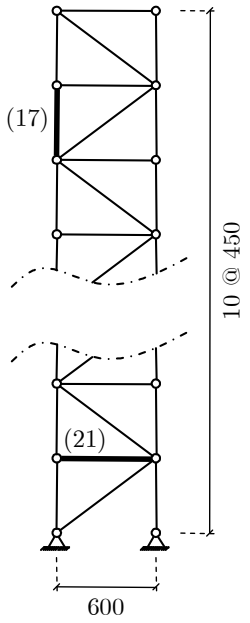

Figure 1: Sketch of the planar truss used for validation purposes; high-frequency contributions are particularly important for the emphasised bars (17) and (21).

3. Extraction of the reduced variances and covariances in the right-hand side of equations (60), and projection of these statistics onto the actual geometrical space of the structure via equations (59).

The numerical solution of equations (61) can be obtained, similarly to those of equations (50), through the following incremental schemes:

$$\mathrm{E}\langle\, \mathbf{x}(t+\Delta t)^{[2]} \,\rangle = \widetilde{\boldsymbol{\Theta}}_2(\Delta t) \cdot \mathrm{E}\langle\, \mathbf{x}(t)^{[2]} \,\rangle + \widetilde{\boldsymbol{\Psi}}_2(\Delta t) \cdot \{\mathrm{E}\langle\, \mathbf{x}(t) w(t) \,\rangle + \mathrm{E}\langle\, \mathbf{x}(t+\Delta t) w(t+\Delta t) \,\rangle\}; \quad (63a)$$

$$\mathrm{E}\langle\, \mathbf{y}(t+\Delta t)^{[2]} \,\rangle = \overline{\boldsymbol{\Theta}}_2(\Delta t) \cdot \mathrm{E}\langle\, \mathbf{y}(t)^{[2]} \,\rangle + \overline{\boldsymbol{\Psi}}_2(\Delta t) \cdot \{\mathrm{E}\langle\, \mathbf{y}(t) w(t) \,\rangle + \mathrm{E}\langle\, \mathbf{y}(t+\Delta t) w(t+\Delta t) \,\rangle\}; \quad (63b)$$

$$\mathrm{E}\langle\, \mathbf{x}(t+\Delta t) \otimes \mathbf{y}(t+\Delta t) \,\rangle = \widehat{\boldsymbol{\Theta}}_2(\Delta t) \cdot \mathrm{E}\langle\, \mathbf{x}(t) \otimes \mathbf{y}(t) \,\rangle + \widehat{\boldsymbol{\Psi}}'_2(\Delta t) \cdot \mathrm{E}\langle\, \mathbf{x}(t) w(t) + \mathbf{x}(t+\Delta t) w(t+\Delta t) \,\rangle + \widehat{\boldsymbol{\Psi}}''_2(\Delta t) \cdot \mathrm{E}\langle\, \mathbf{y}(t) w(t) + \mathbf{y}(t+\Delta t) w(t+\Delta t) \,\rangle. \quad (63c)$$

Transition matrices $\boldsymbol{\Theta}_2$ and loading matrices $\boldsymbol{\Psi}_2$ for the second-order statistics are offered in appendix C.

6. Numerical applications

For the sake of numerical validation, the performances of the proposed DyMAM correction have been tested with the seismic analysis of the 1-bay 10-storey planar pin-jointed truss depicted in figure 1. The structure possesses $n = 40$ DoFs (degrees of freedom), i.e. horizontal and vertical translations of the 20 free joints in elevation. Movements of joints at the same level are not constrained by any deck system (e.g. rigid slab) in parallel with the horizontal bar. For the generic i-th bar of length L_i,

additional lumped masses $M_i = \rho A\, L_i$ have been superimposed at each end to the consistent inertia of the element, so that the total mass of the structure is $M_{\text{tot}} = 1,554$ kg. Geometrical and mechanical data of the structure are given in table 1, while table 2 lists circular frequencies and mass participation ratios of the first six modes of vibration. This objective structure has been chosen because its simplicity may enable one to easily reproduce the results and appreciate the improved accuracy of the proposed strategy of modal correction. It is worth noting here that, analogously to MAM, the larger is the number n of DoFs of the structure under consideration, the more efficient tends to be the DyMAM. Indeed, the number of higher modes of vibration to be retained in the analysis in order to achieve the desired accuracy tends to increase with the number n of DoFs, while the number of dummy oscillators required by the proposed DyMAMcorrection increases with the number ℓ of dynamic excitations.

In a first stage, the FRF have been computed for the axial strain of bars (17) and (21), identified with ticker lines in figure 1. These bars have been selected after a sensitivity analysis, showing that the contribution of higher modes of vibration is particularly important for these two members. Log-log graphs at the top of figure 2 compares the exact FRFs (tick solid lines), computed by retaining all the $m = n = 40$ modes of vibration (and resorting to the damping matrix of equation (24)), with those obtained by modal displacement method (MDM, circles),

Table 1: Truss' geometrical and mechanical data

bay's width	$B = 600$ cm
interstorey's height	$H = 450$ cm
bars' mass per unit length	$\rho A = 2.4$ kg /m
bars' axial stiffness	$EA = 60,000$ KN
modal viscous damping ratio	$\zeta = 0.05$ KN

Table 2: Truss' modal data

mode's number	circular frequency [rad /s]	cumulative mass participation factor [%]
1	8.7	66.0
2	41.8	88.4
3	62.7	88.4
4	92.4	94.9
5	142.7	97.6
6	182.3	97.7

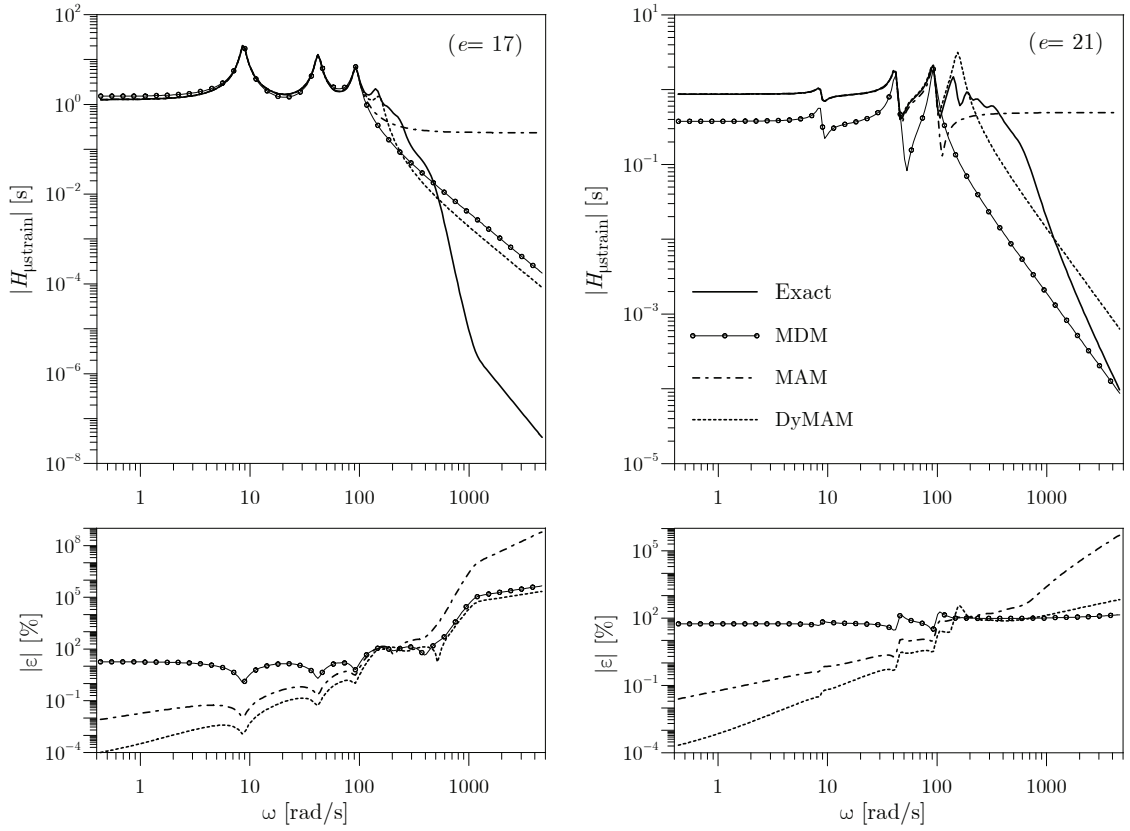

Figure 2: Frequency response function (top) for the seismic-induced axial strain in bars (17) and (21), and percentage inaccuracies of the modal correction methods (bottom).

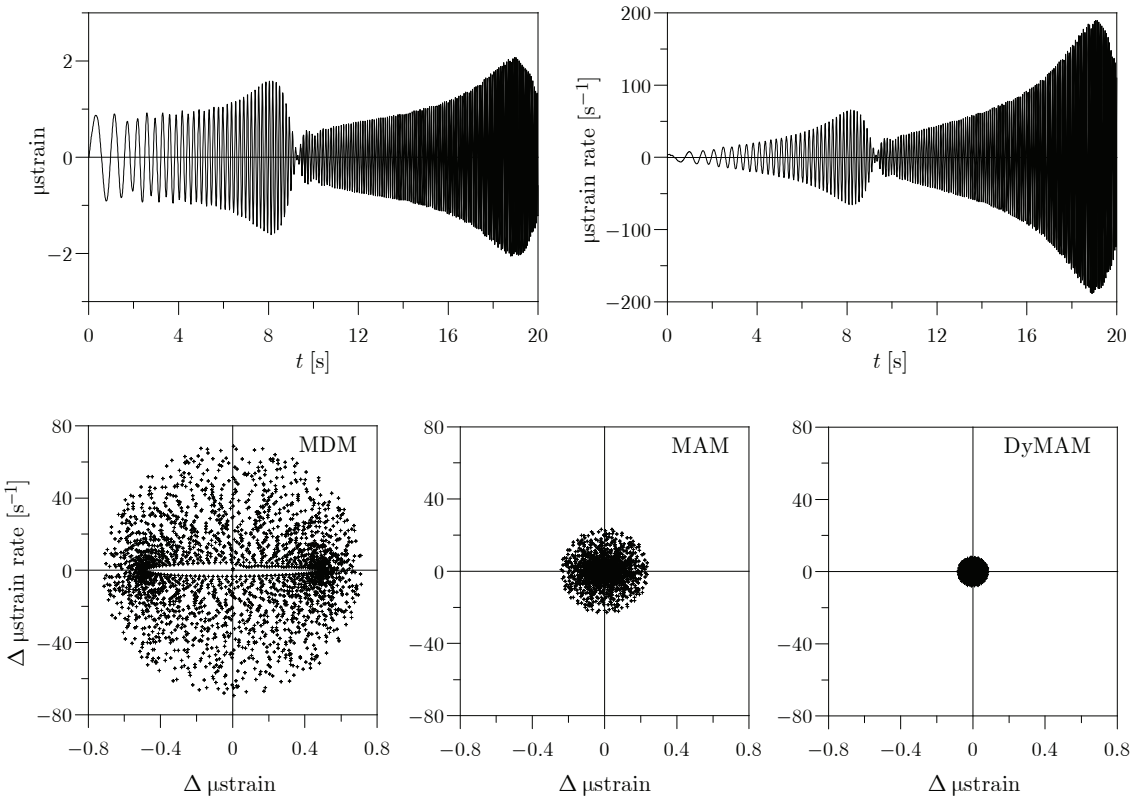

Figure 3: Exact time histories of strain and strain rate (top) and corresponding discrepancies in the phase plane for different modal correction methods (bottom) when just $m = 4$ modes of vibration are retained.

modal acceleration method (MAM, dot-dashed lined) and proposed dynamic MAM correction (DyMAM, dotted lines) when just the first $m = 4$ modes are retained. Interestingly, the modal mass participating in the motion of the structure with $m = 4$ sums up to 94.9% of the total mass (see table 2), i.e. it exceeds the threshold of 90%, which is typically assumed by seismic codes for accepting the truncation. Nevertheless, the inaccuracy of the MDM in the low frequency range is very large. Specifically, at $\omega = 0$ the MDM overestimates the strain in the element $e = 17$ by 35.1%, while the strain in the element $e = 21$ is underestimated by 78.3%. In both cases, the classical MAM correction is able to reduce the inaccuracy in pseudo-static conditions below 0.1%, while the proposed DyMAM further improves the results, with a pseudo-static inaccuracy of the order of 0.0001%. The latter correction is associated with the dynamic response of an additional dummy oscillator having undamped circular frequency $\overline{\omega} = 154.1$ rad/s and viscous damping ratio $\overline{\zeta} = 0.0788$ (as computed by equations (20) and (22), respectively).

The absolute value of the percentage inaccuracy $|\varepsilon|$ against the frequency of vibration ω is plotted in the log-log graphs at the bottom of figure 2. Inspection of these graphs clearly shows that the proposed DyMAM correction performs consistently better than the classical MAM correction. It is particularly important the improved accuracy in the low-frequency range, i.e. $\omega < 100$ rad/s , where most of the energy of dynamic loadings for civil engineering applications is usually concentrated. Interestingly, a small peak appears in the percentage inaccuracy of the DyMAM correction for element $e = 21$ at $\omega \cong 150$ rad/s . This is due to the dynamic amplification of the additional dummy oscillator, whose resonant frequency is $\sqrt{1 - 2\,\overline{\zeta}^2}\,\overline{\omega} = 153.1$ rad/s, and should not be regarded as a pitfall of the proposed approach. Indeed, the resonant frequency of the dummy oscillator is always larger than the highest modal frequency retained in the analysis, i.e. $\overline{\omega} > \omega_m$, which in turn should be larger than the maximum frequency of the dynamic input [9]. The accuracy of the DyMAM correction is guaranteed by satisfying these inequalities.

In a second stage, time-history analyses have been carried out on the objective truss. The seismic input has been selected as a sweep function, able to excites in sequence the first four modes of vibration of the structure:

$$w(t) = \sin\left(\omega_{\mathrm{f}}(t)\, t\right), \tag{66}$$

where:

$$\omega_{\mathrm{f}}(t) = 4.35 + 2.314\, t, \tag{67}$$

and the duration of the forcing function is $t_{\mathrm{f}} = 20$ s. Top part of figure 3 offers the time histories of strain and strain rate for the horizontal bar $e = 21$ as evaluated by considering all the $m = n = 40$ modes, which are virtually exact. Approximate responses obtained with just $m = 4$ modes have been also computed, and the discrepancies with respect to exact responses are depicted in the bottom graphs of figure 3. Being at same scale, a

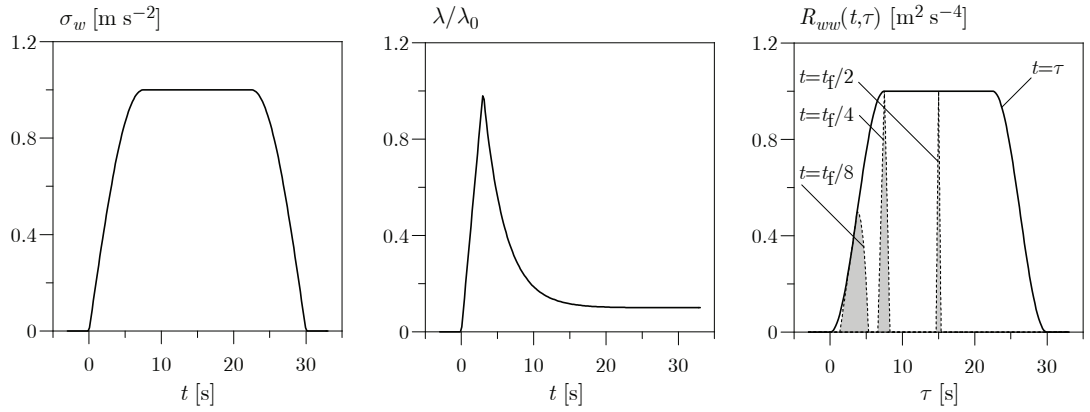

Figure 4: Evolutionary standard deviation (left), correlation time (centre) and auto-correlation function (right) of the random excitation.

visual comparison of these three phase planes is possible, which reveals the inadequacy of the MDM (left), along with the improved accuracy of the proposed DyMAM (right) with respect to the classical MAM (centre). Importantly, it has been possible to correct the strain rate with the MAM just because in this case the input $w(t)$ is given by an analytical waveform, and hence the time derivative $\dot{w}(t)$ of the input is available, while the DyMAM does not suffer from this limitation, being applicable for any input, e.g. recorded accelerograms.

In a third stage, the performances of the proposed DyMAM in presence of random loadings have been investigated. To do so, the ground acceleration $w(t)$ has been modelled as a non-stationary zero-mean Gaussian process, fully defined by the auto-correlation function:

$$R_{ww}(t,\tau) = \sigma_w(\max\{t,\tau\})^2 \left(1 - \frac{|t-\tau|}{\lambda(\max\{t,\tau\})}\right) \cdot \mathrm{U}(\lambda(\max\{t,\tau\}) - |t-\tau|), \tag{68}$$

where time-varying standard deviation $\sigma_w(t)$ and correlation time $\lambda(t)$ of the seismic input are given by:

$$\sigma_w(t) = \begin{cases} 0\,, & t \le 0 \ \vee \ t \ge t_\mathrm{f}\,; \\ \sin(2\pi\, t/t_\mathrm{f})\,, & 0 < t < 0.25\, t_\mathrm{f}\,; \\ 1\,, & 0.25\, t_\mathrm{f} < t < 0.75\, t_\mathrm{f}\,; \\ -\sin(2\pi\, t/t_\mathrm{f})\,, & 0.25\, t_\mathrm{f} < t < t_\mathrm{f}\,; \end{cases} \tag{69a}$$

$$\lambda(t) = \min\left\{t, \lambda_0\left(0.1 + 0.9\,\mathrm{e}^{-10\,(t-\lambda_0)/t_\mathrm{f}}\right)\right\}, \tag{69b}$$

$t_\mathrm{f} = 30$ s being the duration of the stochastic excitation, while λ_0 is the reference value of the correlation time, which has been assumed to be either 3.0 or 0.3 s. Standard deviation, correlation time and auto-correlation function of the seismic input are depicted in figure 4 for $\lambda_0 = 3.0$ s.

It is possible to prove that, for the selected random loading, the input-output cross-correlation functions of equations (62) take the form:

$$\mathrm{E}\langle \mathbf{x}(t)\, w(t)\rangle = \widetilde{\mathbf{\Gamma}}''(\lambda(t)) \cdot \mathbf{f}\, R_{ww}(t,t)\,; \tag{70a}$$

$$\mathrm{E}\langle \mathbf{y}(t)\, w(t)\rangle = \overline{\mathbf{\Gamma}}''(\lambda(t)) \cdot \mathbf{f}\, R_{ww}(t,t)\,. \tag{70b}$$

Knowing the forcing terms in the right-hand side of equations (61), the numerical solutions of equations (63) have been used to evaluate the second-order statistics for the state variables listed in the arrays $\mathbf{x}(t)$ and $\mathbf{y}(t)$, which in turn allow computing the second-order statistics of displacements, strains and stresses in the structure, along with their time derivatives. For illustrative purposes, the evolutionary variance of strain (top graphs) and strain rate (bottom graphs) in the element $e = 21$ of the objective truss are depicted in figure 5 for two reference values of the correlation time of the input. The exact variances obtained with $m = n = 40$ modes are shown with solid lines, while the approximate variances given by classical MDM (i.e. without modal correction) and proposed DyMAM with $m = 2$ (circles), 4 (squares) and 6 (crosses) modes are shown with dot-dashed and dashed lines, respectively. It emerges that the plain MDM heavily underestimates strain and strain rate of the bar, which may lead in practice to unconservative design, particularly for the fatigue limit state. The proposed DyMAM correction is able to greatly improve the results. Specifically, the convergence to the exact variances of the strain is monotonic, and just $m = 4$ modes are enough to gain an excellent agreement with the exact values. The convergence in terms of strain rate is more erratic, although also in this case the DyMAM correction performs much better than the plain MDM. Importantly, the classical MAM cannot be applied directly to the strain rate, since the second-order statistics of the time derivative $\dot{w}(t)$ of the input would be required.

7. Concluding remarks

Practical importance of modal correction methods in the dynamic analysis of linearly-behaving structures has been emphasised, along with the theoretical and computational problems which may arise in the application of existing techniques. Aimed at overcoming these limitations, a novel DyMAM correction, i.e. a dynamic modal acceleration method, has been proposed and numerically validated.

The proposed approach has been initially formulated under the assumption of deterministic dynamic loadings, and successively extended to cope with of random excitations. The basic

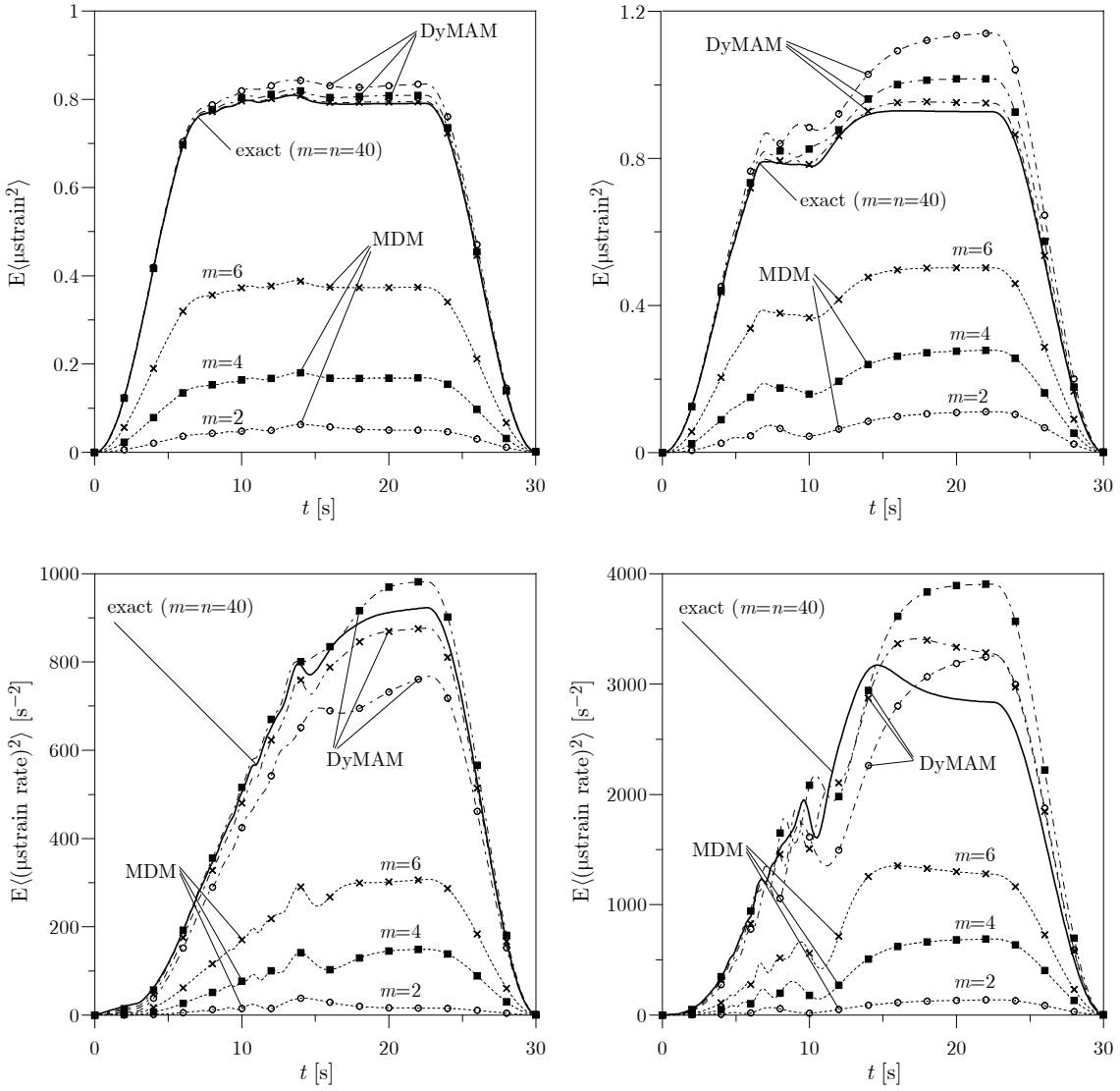

Figure 5: Evolutionary variances of strain (top) and strain rate (bottom) in the element $e = 21$ for long ($\lambda_0 = 3.0$s, left) and short ($\lambda_0 = 0.3$s, right) correlation time of the input.

idea is to introduce an additional dummy oscillator to filter each dynamic loading, and to correct the structural response given by a plain MDM (modal displacement method) with the outputs of these filters. The undamped circular frequency of the dummy oscillators is obtained by applying the machinery of Rayleigh's quotient to the reduced structure, where the contribution of the modes already considered in the MDM is removed, while the viscous damping ratio is computed according to the Rayleigh's damping. Similar expressions have been derived for both discrete and continuous systems, which require the evaluation of reduced flexibility matrix and reduced Greens function, respectively. The Kronecker's algebra has been extensively used to derive in compact form the differential equations ruling the evolution in time of the second-order statistics of the structure vibrating under Gaussian processes. For both problems, efficient step-by-step schemes of numerical solution, and closed form-expressions have been provided for the integration operators. Numerical examples included in the paper demonstrate accuracy and versatility of the proposed DyMAM correction, whose performances are consistently better than those of the very popular MAM (modal acceleration method) correction.

Among the main advantages of the proposed DyMAM: i) ease of implementation, since the corrective term simply involves a set of additional single-DoF oscillators, whose equations of motion are decoupled; ii) simultaneous correction of strain and strain rate, without the need of differentiating the dynamic loadings (like in the MAM, for instance); iii) applicability even in presence of Gaussian processes with an infinite variance (e.g. white noise), while MAM and other techniques fail to do so. Even if specific investigations have not been performed at this stage, it is safe to say that the proposed DyMAM correction is computationally competitive, as the additional burden due to the dummy oscillators is low. Importantly, matrix operations required by the DyMAM are very similar to those of the

classical MAM, and hence the additional memory demand for the corrective term in the proposed technique can be similarly handled.

Further studies will be devoted to extend the DyMAM correction to the seismic analysis of structures with the response spectrum method and to the dynamic analysis of bridge structures subjected to multi-DoF vehicles.

Appendix A. Integration operators (deterministic loads)

This appendix provides closed-form expressions for transition matrix $\widetilde{\boldsymbol{\Theta}}(t)$ and loading matrices $\widetilde{\boldsymbol{\Gamma}}'(t)$ and $\widetilde{\boldsymbol{\Gamma}}''(t)$, which have been used as operators of numerical integration in equation (54a). The expressions of operators $\overline{\boldsymbol{\Theta}}(t)$, $\overline{\boldsymbol{\Gamma}}'(t)$ and $\overline{\boldsymbol{\Gamma}}''(t)$, appearing in equations (54b), can be evaluated similarly.

The transition matrix $\widetilde{\boldsymbol{\Theta}}(t)$, t being the lag time, is by definition the exponential matrix of $\left[\widetilde{\mathbf{D}}\,t\right]$, in which $\widetilde{\mathbf{D}}$ is the matrix of coefficients introduced in the first of equations (51).

This operator can be assembled as:

$$\widetilde{\boldsymbol{\Theta}}(t) = \left[\begin{array}{c|c} \operatorname{diag}\left[\widetilde{\mathbf{h}}(t)\right] & -\widetilde{\boldsymbol{\Omega}}^{-2}\cdot\operatorname{diag}\left[\dot{\widetilde{\mathbf{h}}}(t)\right] \\ \hline \operatorname{diag}\left[\dot{\widetilde{\mathbf{h}}}(t)\right] & -\widetilde{\boldsymbol{\Omega}}^{-2}\cdot\operatorname{diag}\left[\ddot{\widetilde{\mathbf{h}}}(t)\right] \end{array}\right], \tag{A.1}$$

where $\widetilde{\mathbf{h}}(t)$, $\dot{\widetilde{\mathbf{h}}}(t)$ and $\ddot{\widetilde{\mathbf{h}}}(t)$ are the m-dimensional arrays listing the time histories of displacement, velocity and acceleration experienced by the modal oscillators when a unit-step force is applied for $t = 0$. The generic j-th elements of these arrays are known in closed form:

$$\widetilde{h}_j(t) = \widetilde{c}_j(t) + \widetilde{\zeta}_j\,\widetilde{s}_j(t); \tag{A.2a}$$

$$\dot{\widetilde{h}}_j(t) = -\widetilde{\omega}_j\,\widetilde{s}_j(t); \tag{A.2b}$$

$$\ddot{\widetilde{h}}_j(t) = -\widetilde{\omega}_j^2\left(\widetilde{c}_j(t) - \widetilde{\zeta}_j\,\widetilde{s}_j(t)\right), \tag{A.2c}$$

where functions $\widetilde{c}_j(t)$ and $\widetilde{s}_j(t)$ are so defined:

$$\widetilde{c}_j(t) = \cos\left(\widetilde{\Omega}_j\,t\right)\cdot\exp\left(-\widetilde{\zeta}_j\,\widetilde{\omega}_j\,t\right); \tag{A.3a}$$

$$\widetilde{s}_j(t) = \frac{1}{\sqrt{1-\widetilde{\zeta}_j^2}}\cdot\sin\left(\widetilde{\Omega}_j\,t\right)\cdot\exp\left(-\widetilde{\zeta}_j\,\widetilde{\omega}_j\,t\right), \tag{A.3b}$$

with $\widetilde{\Omega}_j = \sqrt{1-\widetilde{\zeta}_j^2}\,\widetilde{\omega}_j$ and $j = 1\ldots m$.

The evaluation of the loading matrices $\widetilde{\boldsymbol{\Gamma}}'(t)$ and $\widetilde{\boldsymbol{\Gamma}}''(t)$ does require simple matrix products:

$$\widetilde{\boldsymbol{\Gamma}}'(t) = \left[\widetilde{\boldsymbol{\Theta}}(t) - \frac{1}{t}\widetilde{\mathbf{L}}(t)\right]\cdot\widetilde{\mathbf{D}}^{-1}; \tag{A.4a}$$

$$\widetilde{\boldsymbol{\Gamma}}''(t) = \left[\frac{1}{t}\widetilde{\mathbf{L}}(t) - \widetilde{\mathbf{I}}_{2m}\right]\cdot\widetilde{\mathbf{D}}^{-1}; \tag{A.4b}$$

where:

$$\widetilde{\mathbf{L}}(t) = \left[\widetilde{\boldsymbol{\Theta}}(t) - \widetilde{\mathbf{I}}_{2m}\right]\cdot\widetilde{\mathbf{D}}^{-1}, \tag{A.5}$$

the inverse matrix $\widetilde{\mathbf{D}}^{-1}$ being known in closed form:

$$\widetilde{\mathbf{D}}^{-1} = \left[\begin{array}{c|c} -\widetilde{\boldsymbol{\Xi}} & -\widetilde{\boldsymbol{\Omega}}^2 \\ \hline \mathbf{I}_m & \mathbf{O}_{m\times m} \end{array}\right]. \tag{A.6}$$

Appendix B. Kronecker's algebra

This appendix offers definitions and properties of the Kronecker's algebra which have been used in formulating the proposed DyMAM correction in presence of random dynamic loadings (section 5).

Let $\mathbf{A}$ and $\mathbf{B}$ be two matrices of dimensions $p\times q$ and $r\times s$, respectively. The Kronecker's product of these two matrices, denoted by $\mathbf{A}\otimes\mathbf{B}$, is the matrix of order $(p\,r)\times(q\,s)$ obtained by multiplying each element a_{ij} of $\mathbf{A}$ by the whole matrix $\mathbf{B}$, that is:

$$\mathbf{A}\otimes\mathbf{B} = \left[\begin{array}{c|c|c|c} a_{11}\mathbf{B} & a_{12}\mathbf{B} & \ldots & a_{1q}\mathbf{B} \\ \hline a_{21}\mathbf{B} & a_{22}\mathbf{B} & \ldots & a_{2q}\mathbf{B} \\ \hline \vdots & \vdots & \ddots & \vdots \\ \hline a_{p1}\mathbf{B} & a_{p2}\mathbf{B} & \ldots & a_{pq}\mathbf{B} \end{array}\right]. \tag{B.1}$$

The Kronecker's product does not enjoy the commutative property, i.e. in general $\mathbf{A}\otimes\mathbf{B}\neq\mathbf{B}\otimes\mathbf{A}$, while when the Kronecker's product is applied to ordinary products of matrices, the following relationship holds:

$$[\mathbf{A}\cdot\mathbf{B}]\otimes[\mathbf{C}\cdot\mathbf{D}] = [\mathbf{A}\cdot\mathbf{C}]\otimes[\mathbf{B}\cdot\mathbf{D}]\,. \tag{B.2}$$

Finally, the k-th Kronecker's power of a matrix $\mathbf{A}$ can be expressed recursively in the following form:

$$\mathbf{A}^{[1]} = \mathbf{A};\quad \mathbf{A}^{[k+1]} = \mathbf{A}^{[k]}\otimes\mathbf{A}. \tag{B.3}$$

Appendix C. Integration operators (random loads)

This appendix offers the expressions for evaluating the integration operators appearing in the differential equations ruling the second-order statistics for the DyMAM correction.

The transition matrices $\boldsymbol{\Theta}_2$ can be computed as Kronecker's square and Kronecker's product of those of the deterministic system [21]:

$$\widetilde{\boldsymbol{\Theta}}_2(\Delta t) = \widetilde{\boldsymbol{\Theta}}(\Delta t)^{[2]}; \tag{C.1a}$$

$$\overline{\boldsymbol{\Theta}}_2(\Delta t) = \overline{\boldsymbol{\Theta}}(\Delta t)^{[2]}; \tag{C.1b}$$

$$\widehat{\boldsymbol{\Theta}}_2(\Delta t) = \widetilde{\boldsymbol{\Theta}}(\Delta t)\otimes\overline{\boldsymbol{\Theta}}(\Delta t). \tag{C.1c}$$

The loading matrices $\boldsymbol{\Psi}_2$ for a one-variate seismic input are given by:

$$\widetilde{\boldsymbol{\Psi}}_2(\Delta t) = \frac{1}{2}\left[\widetilde{\boldsymbol{\Theta}}_2(\Delta t) - \mathbf{I}_{4m^2}\right]\cdot\left[\widetilde{\mathbf{D}}\otimes\mathbf{I}_{2m} + \mathbf{I}_{2m}\otimes\widetilde{\mathbf{D}}\right]^{-1} \cdot\left[\widetilde{\mathbf{V}}\otimes\mathbf{I}_{2m} + \mathbf{I}_{2m}\otimes\widetilde{\mathbf{V}}\right]; \tag{C.2a}$$

$$\overline{\boldsymbol{\Psi}}_2(\Delta t) = \frac{1}{2}\left[\overline{\boldsymbol{\Theta}}_2(\Delta t) - \mathbf{I}_{4\ell^2}\right]\cdot\left[\overline{\mathbf{D}}\otimes\mathbf{I}_{2\ell} + \mathbf{I}_{2\ell}\otimes\overline{\mathbf{D}}\right]^{-1} \cdot\left[\overline{\mathbf{V}}\otimes\mathbf{I}_{2\ell} + \mathbf{I}_{2\ell}\otimes\overline{\mathbf{V}}\right]; \tag{C.2b}$$

$$\widehat{\boldsymbol{\Psi}}_2'(\Delta t) = \frac{1}{2}\left[\widehat{\boldsymbol{\Theta}}_2(\Delta t) - \mathbf{I}_{4m\ell}\right]\cdot\left[\widetilde{\mathbf{D}}\otimes\mathbf{I}_{2\ell} + \mathbf{I}_{2m}\otimes\overline{\mathbf{D}}\right]^{-1} \cdot\left[\mathbf{I}_{2m}\otimes\overline{\mathbf{V}}\right]; \tag{C.2c}$$

$$\widehat{\boldsymbol{\Psi}}_2''(\Delta t) = \frac{1}{2}\left[\widehat{\boldsymbol{\Theta}}_2(\Delta t) - \mathbf{I}_{4m\ell}\right]\cdot\left[\widetilde{\mathbf{D}}\otimes\mathbf{I}_{2\ell} + \mathbf{I}_{2m}\otimes\overline{\mathbf{D}}\right]^{-1} \cdot\left[\widetilde{\mathbf{V}}\otimes\mathbf{I}_{2\ell}\right]. \tag{C.2d}$$

References

1. European Committee for Standardisation, . *Eurocode 8: Design of structures for earthquake resistance*. 2004.
2. Bisplinghoff, R.L., Ashley, H., Halfman, R.L.. *Aeroelasticity*. Cambridge, Mass. USA: Addison-Wesley; 1994.
3. Maddox, N.R.. On the number of modes necessary for accurate response and resulting forces in dynamic analyses. *Journal of Applied Mechanics (ASME)* 1975;**42**:516–517.
4. Schuëller, G., Pradlwarter, H., Schenk, C.. Non-stationary response of large linear fe models under stochastic loading. *Computers & Structures* 2003;**81**(8–11):937–947.
5. Camarda, C.J., Haftka, R.T., Riley, M.F.. An evaluation of higher-order modal methods for calculating transient structural response. *Computers & Structures* 1987;**27**(1):89–101.
6. Akgun, M.A.. A new family of mode-superposition methods for response calculations. *Journal of Sound and Vibration* 1993;**167**:289–302.
7. Borino, G., Muscolino, G.. Mode-superposition methods in dynamic analysis of classically and non-classically damped systems. *Earthquake Engineering and Structural Dynamics* 1986;**14**:705–717.
8. D'Aveni, A., Muscolino, G.. Improved dynamic correction method in seismic analysis of both classically and non-classically damped structures. *Earthquake Engineering and Structural Dynamics* 2001;**30**:501–1517.
9. Di Paola, M., Failla, G.. A correction method for dynamic analysis of linear systems. *Computers & Structures* 2004;**82**:1217–1226.
10. Pesterev, A., Bergman, L.. An improved series expansion of the solution to the moving oscillator problem. *Journal of Vibration and Acoustics (ASME)* 2000;**122**(1):54–61.
11. Biondi, B., Muscolino, G., Sidoti, A.. Methods for calculating bending moment and shear force in the moving mass problem. *Journal of Vibration and Acoustic-Transactions of the ASME* 2004;**126**(4):542–552.
12. Biondi, B., Muscolino, G.. New improved series expansion for solving the moving oscillator problem. *Journal of Sound and Vibration* 2005; **281**(1–2):99–117.
13. Bilello, C., Di Paola, M., Salamone, S.. A correction method for dynamic analysis of linear continuous systems. *Computers & Structures* 2005;**83**(1–2):8–9.
14. Bilello, C., Di Paola, M., Salamone, S.. A correction method for the analysis of continuous linear one-dimensional systems under moving loads. *Journal of Sound and Vibration* 2008;**315**:226–238.
15. Maldonado, G., Singh, M.P., Suarez, L.. Random response of structures by a force derivative approach. *Journal of Sound and Vibration* 1992; **155**(1):13–29.
16. Benfratello, S., Muscolino, G.. Mode-superposition correction method for deterministic and stochastic analysis of structural systems. *Computers & Structures* 2001;**79**:2471–2480.
17. Cacciola, P., Maugeri, N., Muscolino, G.. A modal correction method for non-stationary random vibrations of linear systems. *Probabilistic Engineering Mechanics* 2007;**22**:170–180.
18. Sherman, J., Morrison, W.J.. Adjustment of an inverse matrix corresponding to a change in one element of a given matrix. *The Annals of Mathematical Statistics* 1950;**21**(1):124–127.
19. Caughey, T.K., O'Kelly, M.E.J.. Classical normal modes in damped linear dynamic systems. *Journal of Applied Mechanics (ASME)* 1965; **32**:583–588.
20. Warburton, G.. Rayleigh's contributions to modern vibration analysis. *Journal of Sound and Vibration* 1983;**88**(2):163–173.
21. Di Paola, M.. Moments of non-linear systems. In: *Probabilistic Methods in Civil Engineering - 5th ASCE Specialty Conference*. Blacksburg, US; 2004, p. 285–288.